Investigating Photovoltaic Efficiency and Durability in Low Earth Orbit Through Nanosatellite Payload Design

Dang Nguyen*, Kerry Tang†, Jasper Scherz‡, Ryan McCrory§, Brayden Pallera¶, and Jose Pastrana ‖
Rhodes College, Memphis, TN, 38112

RHOK-SAT is a 1U Nanosatellite, measuring 10 cm x 10 cm x 11 cm. It is a collaborative project between Rhodes College and the University of Oklahoma with the primary scientific mission of characterizing and measuring the degradation of six perovskite solar cells in Low Earth Orbit (LEO) in comparison to a reference ACIGS (Silver-alloyed Copper Indium Gallium Selenide). The RHOK-SAT payload consists of two PCBs: one housing eight Aerospace Measurement Units (AMU) from Aerospace Corporation and a Pogo board, which includes 8 resistance temperature detectors (RTD), a sun sensor, and spring-loaded Pogo pins, a benign method for cell electrical connection. A non conductive, anodized top plate on the top face also acts as the aperture and reduces reflections. Overall, the payload is designed to further the mission's scientific purpose, allowing the collection of as much data as possible in the form of solar cell I-V (Current-Voltage) sweeps, temperature, and sun angles. Furthermore, RHOK-SAT also provides real-world engineering experience to students at Rhodes College, which does not have a formal engineering program. RHOK-SAT will launch in early 2025 on an ISS resupply mission through NASA's CubeSAT Launch Initiative (CSLI) program.

I. Nomenclature

V_{OC}	=	Open circuit voltage
I_{SC}	=	Short circuit current
P_{MP}	=	Max power
FF	=	Fill Factor
R	=	Roll
P	=	Pitch
A	=	Aperture
$V_{TL}, V_{BL}, V_{TR}, V_{BR}$	=	= Voltages of top-left, bottom-left, top-right, bottom-right photo diodes

II. Introduction

The primary engineering challenge of RHOK-SAT lies in designing, calibrating, and protecting experimental devices and hardware while accommodating the limited payload space onboard. The specific architecture we are using, ISISpace, includes an internal PCB stack that maintains core operation, leaving minimal space for our payload. These constraints highly influenced many of our choices regarding physical materials and electronic components, each having to maximize the given space without compromising functionality. Such limitations are common in CubeSAT missions. However, we chose to focus on novel photovoltaic cells due to their potential to generate power. While promising, they also introduce their own set of challenges. In this paper, we outline our approach to addressing these challenges to achieve a balance between space efficiency, durability, and operational capacity.

---

*Undergraduate Physics Major, Department of Physics, 2000 North Parkway, and AIAA Student Member 1424774

†Undergraduate Computer Science Major, Department of Computer Science, 2000 North Parkway, and AIAA Student Member 1811100

‡Undergraduate Physics Major Math Double Major, Department of Physics Department of Math, 2000 North Parkway, and AIAA Student Member 1823566

§Undergraduate Physics Major, Department of Physics, 2000 North Parkway, and AIAA Student Member 1823387

¶Undergraduate Physics Major, Department of Physics, 2000 North Parkway, and AIAA Student Member 1823567

‖Graduate Lead Engineer and Advisor, Department of Computer Science, 2000 North Parkway, and AIAA Young Professional 773676

III. Photovoltaic Materials

Our goal is to understand the performance of photovoltaic materials in the extreme conditions of space. This section details our approach to how we plan to evaluate their efficiency and durability while also addressing the challenges of obtaining accurate measurements in such a harsh environment.

A. I-V Curve

First, we chose to focus primarily on the I-V curve. These curves will take a form similar to that of 1 after measurement. [1] This curve is essential to understanding the electrical characteristics of our cells as it provides valuable insights in several key parameters.
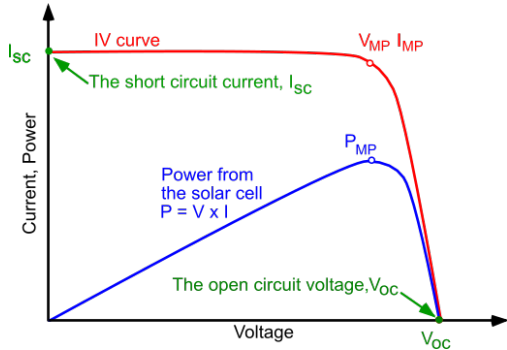
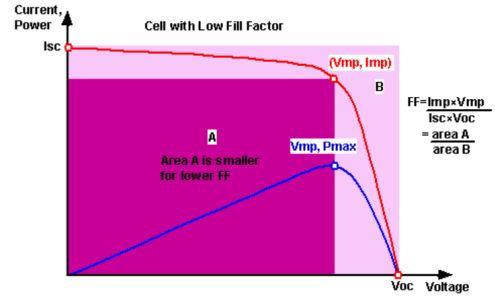
Fig. 1   Example I-V Curve of a Solar Cell

Fig. 2   Fill Factor Calculations

The first points of interest when looking at a solar cell's I-V curve are its two intersections with the voltage axis (V_{OC}) and the current axis (I_{SC}). Along the graph, there is also a specific point P_{MP} where the power produced by the solar cell reaches its maximum value. The fourth parameter that can be interpreted from the I-V curve is the ratio between P_{MP} and the product of V_{OC} and I_{SC} called FF. The higher the resulting FF, in other words, the steeper and more abrupt the IV curve fell off at the tail end of the measurement, the healthier a solar cell. Two types of resistance, series and shunt resistance, are common causes of FF loss, and reducing them was essential for optimization. In selecting our final flight cells, we tried to focus on all of these key factors.
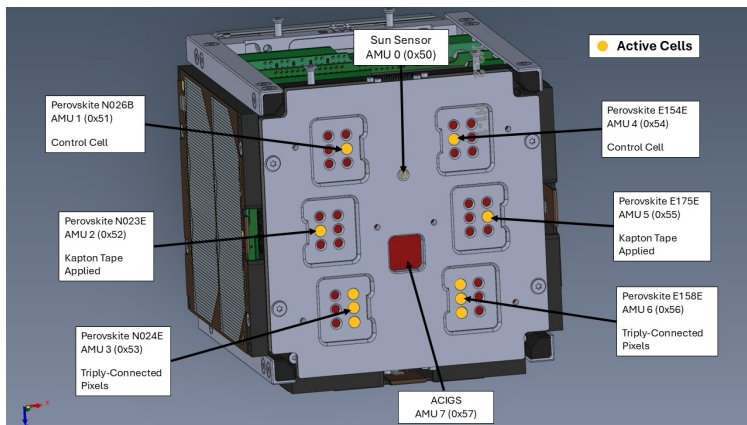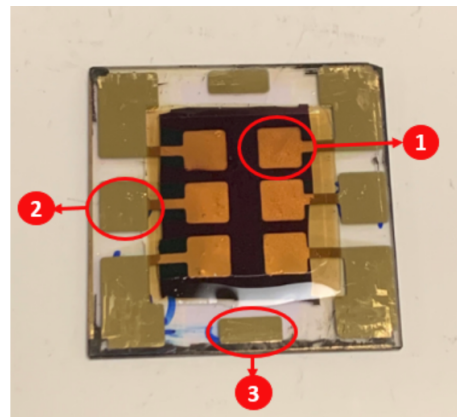
B. Perovskites

Fig. 3   Labeled top plate

Fig. 4   Sample Perovskite Device
1. Active Perovskite Area
2. Negative Electrode
3. Common Positive

Perovskites are the main research focus of this project and are a novel photovoltaic material that has many exciting characteristics, boasts a higher theoretical efficiency than conventional silicone materials, is relatively inexpensive and fast to produce by printing on glass substrates, and exhibits a high radiation tolerance as seen in both Ref. [2] and Ref. [3], and even has a self-healing property.[4] The structure of the perovskite can be seen in figure 4 with each active device area or individual sub-cell of a sample being called a "pixel." Interfacing with these pixels is our main concern if we want to explore their capabilities. Unfortunately, perovskites are also a very finicky material as they are particularly sensitive to moisture. Prolonged exposure to heat produced by solder and contact with chemicals such as epoxies can also damage the crystalline structure, making it difficult to mount the structures. Nevertheless, perovskites seem to have a bright future in aerospace applications, which we plan to explore with our payload while navigating its limitations.
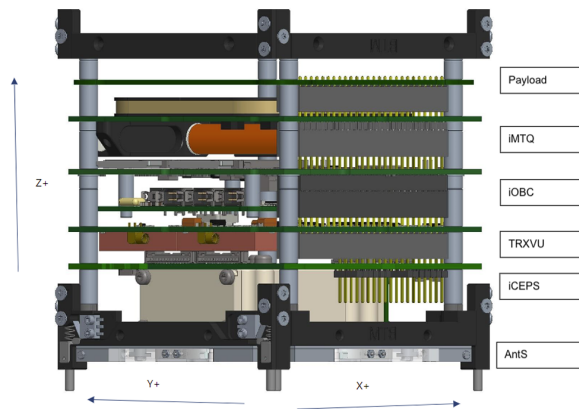
IV. Payload Overview

Fig. 5   RHOK-SAT's Internal PCB Stack

Situated on the +Z face and the top 2.8 mm of the satellite's internal PCB stack as shown in figure 5, RHOK-SAT's payload consists of two main electromechanical assemblies: the "Sandwich" 6 and the AMU board. 10 What we call the "Sandwich," replacing the +Z solar panel of the CubeSAT, is our densely packed solution to the requirement that the perovskites must be dry mounted. On the base of the sandwich is the Pogo board, named after the 48 spring pins (pogo pins) soldered to establish a connection to the cells. The perovskite cells are then compressed down to the pins and held in place by the aluminum top plate, the top layer of the sandwich. Between the two layers are the rest of the experimental devices, including one sun sensor to keep track of the angle of the top plate to the Sun, one ACIGS cell, a more conventional photovoltaic material used as the control, the six perovskite solar cells, and eight RTDs to measure the internal temperature of the various cells in orbit.

Underneath the sandwich in the internal PCB stack is the AMU board, 10 which houses the measurement devices developed by the Aerospace Corporation. We intentionally soldered four on both sides to make full use of the space. The construction of an AMU board is simple and consists of three main connections: a few rows of header pins on the CubeSAT Kit Bus (CSKB), the AMU solder points, and a Molex flexible wire connector to our Pogo Board. [5] We deliberately chose the 60-pin Molex connector as it allowed us to achieve multiple connections within a single Molex cable. [6] The CSKB connects all the CubeSAT's electrical systems and powers our AMUs while communicating to the software via I2C, a serial communication protocol.
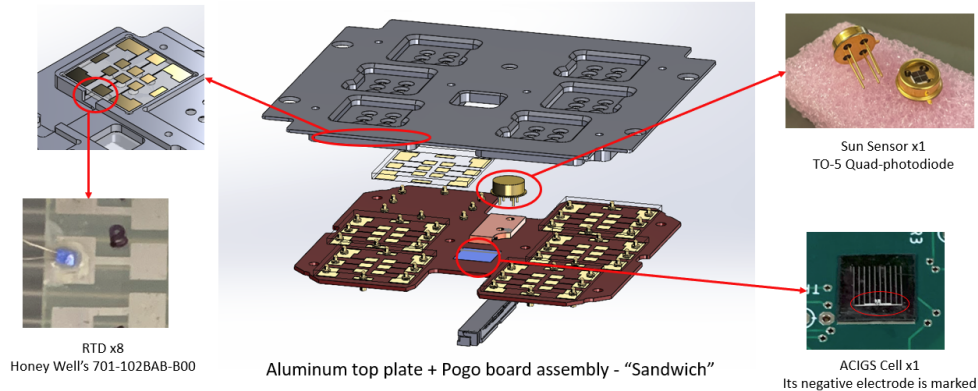
V. The "Sandwich"

Sun Sensor x1
TO-5 Quad-photodiode

Aluminum top plate + Pogo board assembly - "Sandwich"

RTD x8
Honey Well's 701-102BAB-B00

ACIGS Cell x1
Its negative electrode is marked

Fig. 6   The "Sandwich" and Its Components

A. Pogo Board

To overcome the distinct limitations of each experimental device needed to achieve the scientific mission of RHOK-SAT, we devised two methods: Pogo pins and the P-Connector.
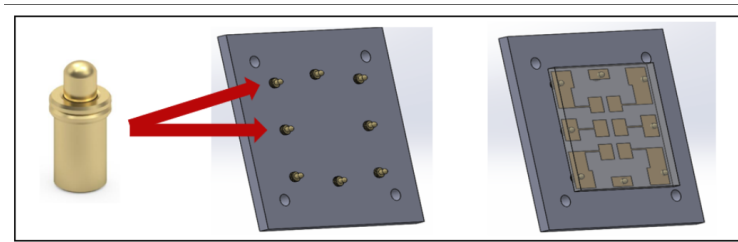

Fig. 7   Pogo Pins Connection Scheme to a Perovskite Slide

Vulnerabilities of the perovskites, such as excess heat and moisture, will rule out most conventional mounting methods such as glue, tape, or solder. Thus, the team selected gold coated, spring-loaded pogo pins to act as a benign method for electrically connecting the cells to our satellite. 7 This was simple and extremely effective.

For the ACIGS cell, the main challenge is to accommodate its particular design with the limited space we have on the Sandwich. The ACIGS material is printed on a small (10 x 10 mm) stainless steel piece with a thickness of only a few microns. Thus, we would have to be creative. First, to electrically connect to the positive electrode, the cell's back side, we selected a conductive epoxy, specifically Ref. [7], to bond the cell directly onto a surface mount on the Pogo board. To mount onto the negative, the horizontal line on the surface of the cell, we designed and manufactured a P-shaped copper piece called the P-connector. 8 One distinctive element of the P-connector is the teeth at the end, which allow it to make contact with the cell while avoiding its edges and preventing the cell from short circuiting. To attach it, we countersunk a hole on the Pogo board to place a screw underneath the Molex connector which maintains pressure with the board and the connector. 6

Lastly, to mount the RTDs on the devices, we used an electrically insulating, thermally conductive, and elastic thermal paste. [8] Six RTDs are mounted directly on the glass substrate of the perovskite devices opposite the material side. The seventh RTD used to monitor the ACIGS cell is mounted on the side of the P-connector instead of directly onto the cell. The last RTD is mounted directly on the top plate, near the sun sensor. 6
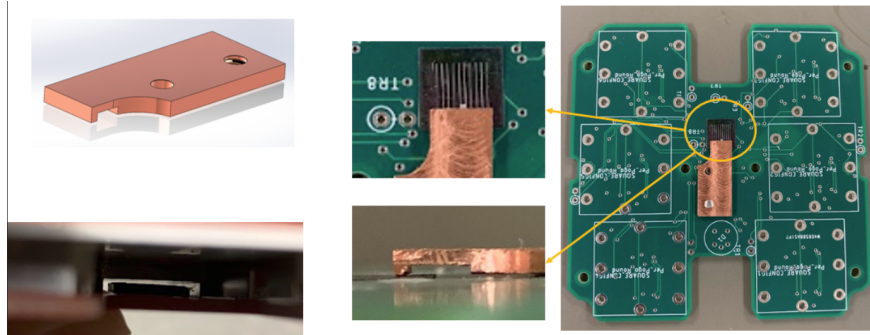
Fig. 8   P-Connector Design and Integration

B. Top Plate

1. Design

The team designed the aluminum face plate with the intention of maximizing the number of perovskite samples that could be mounted on the payload face of the satellite while still maintaining a low profile and minimized volume. The face plate has a total of six square pockets, one for each perovskite device. Each pocket has six aperture holes above the six pixels on each device to restrict sunlight, ensuring a consistent area of illumination across all perovskite samples. Another small aperture hole sits directly above the sun sensor to restrict its field of view and limit stray light that interferes with sensor readings. The solar cells receive the most sunlight and produce the most power when the Sun is perpendicular to the cells. As the Sun will only occasionally be perpendicular to the payload face, a maximum angle of 35 degrees from perpendicular to the payload face was deemed adequate. The sun sensor will thus have a 70 degree field of view from the aperture. Note, this is the mechanical field of view, but the actual field of view, we will explore later, is more restricted.
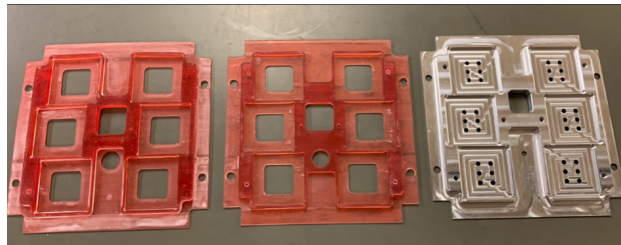

Fig. 9   From Resin Prototype to Aluminum Top plate [9]

2. Fabrication

The fabrication of the top plate consists of two phases: prototyping with 3D resin printing and CNC machining. To minimize error, time, effort, and material, all iterations of the top plate CAD model would go through several rounds of prototyping with 3-D resin printing 9 before being machined. After the resin print is ready, it will be used for various tests, including fitment tests to troubleshoot physical interference with other payload PCBs or the CubeSAT frames and rough solar cell - sun sensor sweeps to alter, adding, or verify smaller design elements like the various aperture holes. For the CNC process, the parts that will be flown into orbit must be precisely machined to tight tolerances out of aerospace-grade aluminum. Thus, it is made out of aluminum 6061, an aluminum alloy known for its high machinability and corrosion resistance. [10]

The CAD file of the top plate is imported from SolidWorks into Autodesk Fusion 360 CAM software for the machining process, using the HAAS Mini-Mill, a 3-axis CNC machine located in the Rhodes College machine shop. Each top plate takes around three to four hours for the CNC mill to complete manufacturing. Many of the cutting operations must be performed in slow cutting paths to protect the thin plate from harmful vibrations and warping that can occur during the machining process. Another way to protect the part and the cutting tools is to use the right tool

made of the right material. To prolong the life of cutting tools, they can also be coated in materials such as titanium nitride (TiN) and titanium carbonitride (TiCN). These coatings increase the durability of the cutting tools, allow for a faster cutting speed, and produce a finer cut in the aluminum. The tools required for the precise machining of the aluminum are carbide tools coated in TiCN. After the faceplate is fabricated, it must be anodized to protect it from space conditions. The process of anodizing creates a strong layer of corrosion resistance that cannot be chipped off for the aluminum surface. Anodization also gives the top plate a insulating property, which is crucially important in preventing perovskite devices from falling apart once they are inside the pocket of the plate. It also makes it non-reflective, which may reduce stray reflections that could impact readings. Overall, there is still more to the Sandwich, but this outline the main challenges and solutions regarding the hardware components.
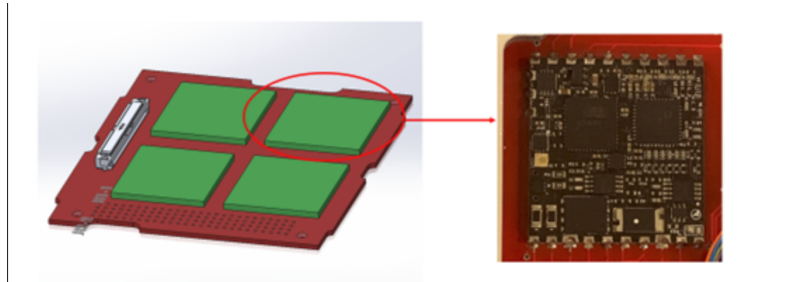
VI. AMU Board

Fig. 10   AMU PCB

Beneath the Sandwich is where the AMU board lies. An AMU, developed by the Aerospace Corporation, is the integrated circuit that we are using to characterize the photovoltaic cells. We chose seven out of the eight AMUs on board to measure the perovskites and ACIGS and dedicated the last to trigger sweeps and collect angle measurements from the Sun sensor. The eight AMUs are also connected to their own 1000-ohm platinum RTD.[11] By applying a current to the RTDs, the AMU measures a voltage and calculate a resistance, which maps to a temperature. The AMUs also include a Metal-Oxide-Semiconductor Field Effect Transistor (MOSFET) HTR pin, which our team has dedicated to activate or deactivate the sweep circuit. To ensure its accuracy, with the help of a representative from Aerospace Corporation, we calibrated the AMUs through a procedure involving the Keithley 2400 and two calibrated bench-top multimeters for both voltage and current. Due to their versatility, AMUs are a critical part in facilitating communication between the satellite and the rest of our circuit. This circuit can be broken down into two parts: the measurement circuit and the resistor circuit.
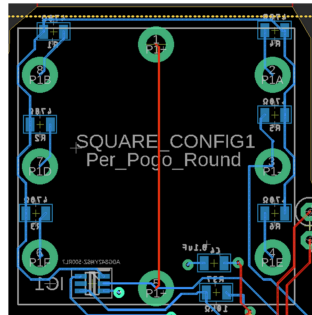
VII. Circuitry

Fig. 11   Example of the Circuit in a Single Slot (Designed using EAGLE CAD)

A. Measurement Circuit

At its core, to perform an I-V sweep, the AMU takes a 4-wire measurement shown in Ref. [12] of the current/voltage through an internal variable resistor. At high resistance, it measures V_{OC} and continues consecutive measurements before reaching I_{SC} with minimal resistance. Following this principle, the core of the measurement circuit involves a four-wire connection scheme across a pixel. We accomplished this by connecting the Pogo pins' common positive to the AMU's positive terminal and negative pins to the AMU's negative. The same idea applies to measure the ACIGS. With this configuration, the AMUs can perform I-V sweeps with our devices. Thus, this is repeated for each of the 6 sample slots on the Pogo board. 11

Note that a large portion of our time was dedicated to exploring an 8-channel multiplexer. [13] Rather than only six pixels in six samples, we could have measured 36 pixels in six samples with the same number of AMUs. RHOKSAT's channel bus lines would allow manipulation of a bit field corresponding to binary input of the select lines that isolate any particular pixel. However, through rigorous testing and redesigns, we noticed crosstalk between pixels that threatened the reliability of our data. Thus, it was scrapped. A possible theory is that the multiplexers used impedance to switch the analog signals, thus not truly isolating. Emails to Oscilla suggested that reed relays could have worked since they would physically isolate the signal. However, the specific electronic part they suggested was too large, and moving parts tend to be discouraged in space. [14] Nevertheless, by prioritizing one pixel per sample, our circuit design was simplified and made easier to execute. We learned a lot from that approach, but in our short timeline, it made sense to consider that less is sometimes more.
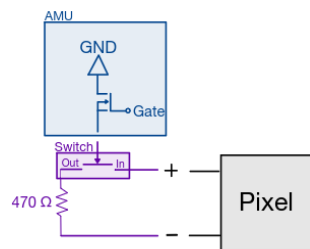
B. Resistor Circuit

Fig. 12   Labeled Resistor Circuit

One challenge we had to work around is the fact that perovskites, left exposed to light, will degrade if there is no load to discharge. Thus, we must keep the unmeasured pixels alive to keep the entire sample alive. In addition to covering the unused pixels with silver Kapton to avoid unnecessary light exposure, we designed a resistor circuit. This circuit uses a switch to switch the pixels to their 470 ohm resistive load. We chose this particular resistance value as we calculated it to be an average resistance where peak power occurs. To accomplish this, we chose an inverted switch from Ref. [15] with default state ON, requiring no additional power, apart from the 3.3 V of the switch itself to keep active. This switch is controlled by activating or deactivating AMU's HTR pin. Originally, this design was implemented with all the pixels. However, through numerous tests, we discovered that the switch also would not isolate the signal as we wanted. Therefore, disengaging the switch to allow the measurement circuit to take part would lead to visible shunt resistance in the curves, which we mentioned earlier that is detrimental to FF. Thus, we removed the one resistor on the measured pixel. This is not ideal, but we considered the compromise because of the perovskite's self-healing nature and the fact that the other pixels were covered. Additionally, if the cells were exposed to light, we would always be measuring that single pixel regardless. Other ways to allow the cell to discharge could be through the AMU's internal resistor. However, this would not be a passive circuit, requiring the AMU on at all times to control the resistance value. This same play between measurement, power, and light is what we also focus on when it comes to integrating our sun sensor.

VIII. Sun Sensor

Unlike a Keithley 2400 SMU, which is a source meter capable of applying its own voltages to measure cells, the AMU is a passive circuit that relies on the cell's voltages. This distinction is important and comes into play when considering our emphasis on integrating and calibrating a Sun sensor with the setup. The role of the Sun sensor is to act as a trigger for the measurement procedure when light is within an angle threshold. Before, we mentioned that the Sun
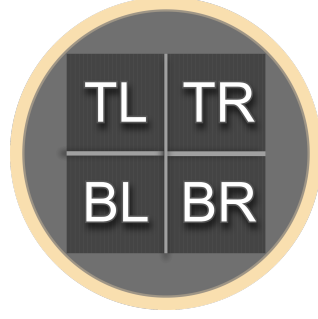
Fig. 13 Labeled Quad Photo Diode

sensor is on its own AMU. We neglected to mention that it also has its own power line. By separating the triggering mechanism from the rest of the measurement circuit, we can turn on the measurement AMUs only when necessary, thus reducing unnecessary power consumption, which is crucial for longevity in space. In particular, RHOK-SAT uses a TO-5 quad photo diode with a blackened photoetched aperture. The AMU allows us to measure the voltages of each of its four diode quadrants, which will help determine where the Sun's light is angled relative to the satellite's top plate. The ideal angle is $\theta = 0$, where the expected power generation of the perovskite cells should be at its maximum.

Before determining the angular position of the top plate, there are a few intermediary steps. These are determined by the series of formulas mentioned below, which are automatically calculated onboard the AMU's firmware through measurement data and coefficients stored in its read-only memory (EPPROM). The first are the voltage ratios in the roll and pitch angles, which correspond to Figure 13 and the equations 1 and 2. Intuitively, these make sense as roll is calculated through the left minus the right quadrants, the same idea for pitch with top minus bottom. Dividing by the total acts to normalize the data.

$$R_{Ratio} = \frac{(V_{TL} + V_{BL}) - (V_{TR} + V_{BR})}{V_{TL} + V_{TR} + V_{BL} + V_{BR}} \tag{1}$$

$$P_{Ratio} = \frac{(V_{TL} + V_{TR}) - (V_{BL} + V_{BR})}{V_{TL} + V_{TR} + V_{BL} + V_{BR}} \tag{2}$$

To map these voltage ratios to angles, they are then multiplied by an aperture ratio of the aperture radius (RVAL) and height (HVAL) 3 and put through an arc tangent through equations 4 and 5, respectively.

$$A_{Ratio} = \frac{HVAL}{RVAL} \tag{3}$$

$$R_{ATAN} = \arctan\left(R_{Ratio} * A_{Ratio}\right) \tag{4}$$

$$P_{ATAN} = \arctan\left(P_{Ratio} * A_{Ratio}\right) \tag{5}$$

At this point, there is no guarantee that the angles will match real-life conditions. Therefore, a calibration procedure is required to add a correction. There are many ways to approach this, many of which the team tried. For instance, we created a flat-SAT that simulates CubeSAT's sandwich without the satellite, attached it to a two-axis jig with a protractor underneath a solar simulator, and inputted angle data by hand. This, while meticulous, seemed promising, but differences in the Sun's collimated (parallel) light with the Oscilla solar simulator's uncollimated light proved worrisome. Instead, another approach involved using the actual Sun. By matching RHOK-SAT's Sun sensor with an already corrected Sun sensor, the process could be automated with software as long as both sensors received the same exposure to light. This is what the team eventually went with.

Thus, the team designed a 3-D fixture 14 to mount RHOK-SAT's flat-SAT parallel to EYAS, which is another AMU payload originally sent on a balloon mission to measure solar cells on the edge of space. [16] With the AMU development board for I2C communication, the team wrote an Arduino program that captured raw diode data from both Sun sensors simultaneously, so that the uncorrected Sun sensor's angles could be mapped to the EYAS's corrected angles. Subsequent data analysis interpreted the data as Pandas data frames, which allowed the use of IQR and -30 to 30 degree filters to clean the data, remove outliers, and isolate the usable range that our threshold will be under. Then, by plotting RHOK-SAT's arc-tan values on the x-axis and EYAS's corrected values on the y-axis, we apply polynomial
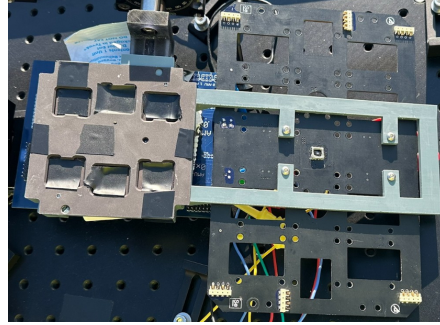
Fig. 14 Sun Sensor Calibration Mount - Flat-SAT (left), EYAS (right)

regression to get the final third-order fit. The coefficients (A, B, C, D) of which we will use to correctly map our values to EYAS. Note equations 6 and 7. By setting these coefficients for both roll and pitch in the AMU's EPPROM, the AMU could simply input angles into this polynomial function to obtain the corrected roll and pitch. Finally, by treating this roll and pitch as vector components, θ, the magnitude of the resultant vector, becomes our returned value: the Sun angle. 8

$$\mathbf{R} = Ax^3 + Bx^2 + Cx + D \tag{6}$$

$$\mathbf{P} = Ax^3 + Bx^2 + Cx + D \tag{7}$$

$$\theta = \sqrt{\mathbf{R}^2 + \mathbf{P}^2} \tag{8}$$

IX. Vibration Test

Fig. 15 RHOK-SAT in the deployer while mounted on a vibration apparatus, simulating conditions satellite will experience in Cygnus while en route to the ISS.

Once the team integrated the entire Sandwich onto RHOK-SAT and applied permanent Loctite to every screw and bolt, it was time for the final test: the Vibration test, or "Vibe" test. We had to exercise great care during the disassembly and reassembly processes of RHOK-SAT to prevent the frame and the PCB stack from tilting, ensuring the satellite's profiles to remain as square as possible. Additionally, if a single screw became loose during vibration, whether during a simulated test or a real launch into space, the satellite would either not have a guaranteed spot on the rocket or not survive the trip. Thus, with great tension and a full 24-hour wait to allow the thread locker to completely cure, the team and RHOK-SAT departed to a Nanoracks office in Huntsville, Alabama. The night before, a mission manager performed various quality inspections, including checking frame tolerances with the deployer. 17 This included putting the ABFs, so that the satellite was in a deployable state, the exact conditions while aboard the rocket. RHOK-SAT was then mounted to a mock deployment system along with a deployment spring and spacer. 18 The next day, the team took the mock deployer with RHOK-SAT still inside to a testing facility. Here, RHOK-SAT was subjected to specific frequencies and amplitudes required by the ISS along three axes (X, Y, Z). If the satellite survived with solar cells still intact, we can have full confidence that the final assembly will survive the conditions of launch into orbit 15 Ultimately, the satellite passed the vibration test intact, with all the experimental hardware and satellite subsystems still functioning as intended. At that point, hardware is officially locked in and no more physical changes would be made until its launch

to orbit. Currently, RHOK-SAT is ready for handover and integration to the real Nanoracks deployment system in Houston, Texas, this late March.
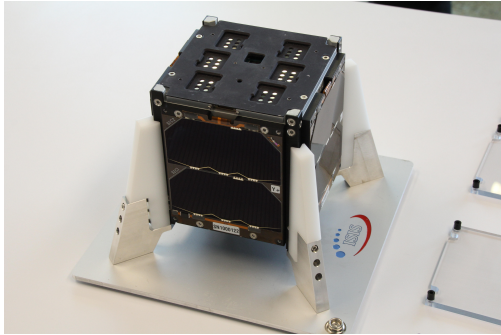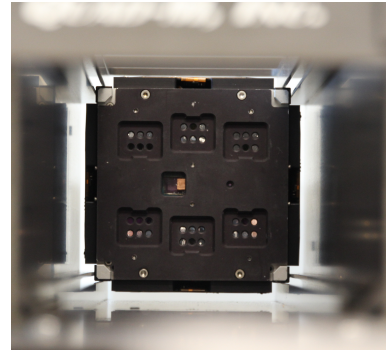

Fig. 16   Flight Model

Fig. 17   Looking down Cube-SAT deployer with RHOK-SAT installed

Fig. 18   Nanoracks Deployer with Panels Removed

Acknowledgments

References

[1] Honsberg, C. B., and Bowden, S. G., "IV Curve," , 2019. URL `https://www.pveducation.org/pvcdrom/solar-cell-operation/iv-curve`, accessed: 2025-03-03.

[2] Durant, B. K., Afshari, H., Singh, S., Rout, B., Eperon, G. E., and Sellers, I. R., "Tolerance of Perovskite Solar Cells to Targeted Proton Irradiation and Electronic Ionization Induced Healing," *ACS Energy Letters*, Vol. 6, No. 7, 2021, pp. 2362–2368. https://doi.org/10.1021/acsenergylett.1c00756.

[3] Miyazawa, Y., Ikegami, M., Chen, H.-W., Ohshima, T., Imaizumi, M., Hirose, K., and Miyasaka, T., "Tolerance of Perovskite Solar Cell to High-Energy Particle Irradiations in Space Environment," *iScience*, Vol. 2, 2018, pp. 148–155. https://doi.org/10.1016/j.isci.2018.03.020, URL https://www.sciencedirect.com/science/article/pii/S2589004218300294.

[4] Afshari, H., Chacon, S. A., Sourabh, S., Byers, T. A., Whiteside, V. R., Crawford, R., Rout, B., Kirmani, A. R., Luther, J. M., Eperon, G. E., and Sellers, I. R., "Triple Halide Perovskite Solar Cells with Thermal Stability over 200 °C with Radiation Tolerance and Self-Healing," *AIP Advances*, Vol. 1, No. 2, 2023, p. 026105. URL https://pubs.aip.org/aip/ape/article/1/2/026105/2910485/Radiation-tolerance-and-self-healing-in-triple.

[5] Molex, "2004850660 Molex Connector," , 2023. URL https://www.molex.com/en-us/products/part-detail/2004850660.

[6] Molex, "5051106096 Cable," , 2023. URL https://www.digikey.com/en/products/detail/molex/5051106096/6099635, accessed: 2025-03-12.

[7] MasterBond, "EP21TDCS-LO Epoxy Adhesive," , 2023. URL https://www.masterbond.com/tds/ep21tdcs-lo.

[8] MasterBond, "EP21TDCS-2LO," , 2023. URL https://www.masterbond.com/tds/ep21tdcs-2lo.

[9] Nguyen, D., "2023 SPS Chapter Research Award - Rhodes College," , 2023. URL https://www.spsnational.org/awards/sps-chapter-research-award/2023/rhodes-college.

[10] Association, A., Davis, J., and University, P. S., *Aluminum Alloys*, Washington D.C. and Materials Park, 1994 and 1993 and 2025. URL https://sites.esm.psu.edu/courses/emch13d/design/design-tech/materials/aluminum_alloys.html.

[11] Honeywell, "700 Series RTD Temperature Sensors," , 2023. URL https://automation.honeywell.com/us/en/products/sensing-solutions/sensors/temperature-and-humidity-sensors/rtd-sensors/700-series#overview.

[12] Research, C., "4-Wire Testing," , 2025. URL https://www.camiresearch.com/Campaigns/Web-Articles/4-wire-testing.html.

[13] Instruments, T., "TMUX1108 – Low-Leakage, 8:1, 1-Channel Multiplexer," , 2025. URL https://www.ti.com/product/TMUX1108.

[14] Teverovsky, A., "Relay Failures Specific to Space Applications," Tech. rep., NASA Electronic Parts and Packaging (NEPP) Program, 1999. URL https://nepp.nasa.gov/DocUploads/C488690C-C4EA-4A27-8245C285D897EC3F/Relay-failure.pdf.

[15] Devices, A., "ADG842: 1 CMOS, Low Voltage, SPST Switch," , 2025. URL https://www.analog.com/en/products/adg842.html.

[16] Corporation, T. A., "Testing Solar Cells at the Edge of Space," *The Aerospace Corporation*, 2019. URL https://aerospace.org/article/testing-solar-cells-edge-space.